Nanoscale

Accepted Manuscript

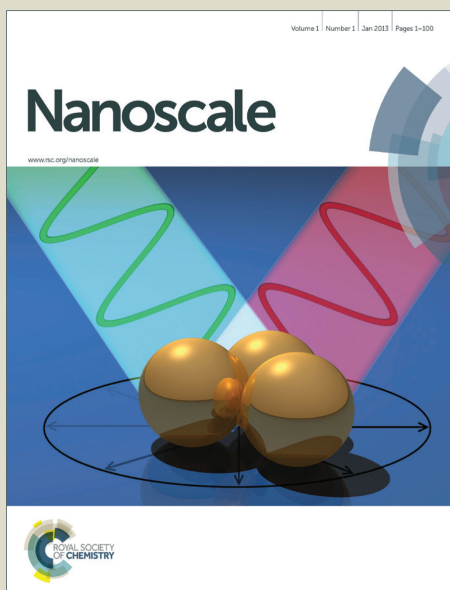

This is an *Accepted Manuscript*, which has been through the Royal Society of Chemistry peer review process and has been accepted for publication.

Accepted Manuscripts are published online shortly after acceptance, before technical editing, formatting and proof reading. Using this free service, authors can make their results available to the community, in citable form, before we publish the edited article. We will replace this *Accepted Manuscript* with the edited and formatted *Advance Article* as soon as it is available.

You can find more information about *Accepted Manuscripts* in the Information for Authors.

Please note that technical editing may introduce minor changes to the text and/or graphics, which may alter content. The journal's standard Terms & Conditions and the Ethical guidelines still apply. In no event shall the Royal Society of Chemistry be held responsible for any errors or omissions in this *Accepted Manuscript* or any consequences arising from the use of any information it contains.

ROYAL SOCIETY OF CHEMISTRY

www.rsc.org/nanoscale

Nanoscale RSCPublishing

COMMUNICATION

Highly Conducting Graphene Film with Dual-Side Molecular n-Doping

Cite this: DOI: 10.1039/x0xx00000x

Youngsoo Kim,[a,b†] Jaesung Park,[c,d†] Junmo Kang,[e] Je Min Yoo,[a] Kyoungjun Choi,[a] Eun Sun Kim,[a] Jae-Boong Choi,[e] Chanyong Hwang,[c] K. S. Novoselov[d] and Byung Hee Hong[a*]

Received 00th January 2012,
Accepted 00th January 2012

DOI: 10.1039/x0xx00000x

www.rsc.org/

Doping is an efficient way to engineer the conductivity and the work function of graphene, which is, however, limited to wet-chemical doping or metal deposition particularly for n-doping, Here, we report a simple method of modulating the electrical conductivity of graphene by dual-side molecular n-doping with diethylenetriamines (DETAs) on top and amine-functionalized self-assembled monolayers (SAMs) at bottom. The resulting charge carrier density of graphene is as high as -1.7× 10^{13} cm^{-2}, and the sheet resistance is as low as ~86 ± 39 Ω/sq, which is believed to be the lowest sheet resistance of monolayer graphene reported so far. This facile dual-side n-doping strategy would be very useful to optimize the performance of various graphene-based electronic devices.

Introduction

Graphene is an atom-thick material with honeycomb lattice structures consisting of sp^2 bonded carbons,[1] which has been intensively studied owing to its fascinating 2-dimensional properties including flexibility,[2] ultrahigh mobility,[3] high transparency[4] and outstanding heat dissipating ability[5] useful for various electronic and optoelectronic applications.[6] Among these properties, the electrical tunability based on its unusual band structure[1] enables the optimization of the electrical conductivity and the work-function of graphene, which is important for various conducting electrode applications.[7] Doping is one of the efficient methods to control the electrical properties of graphene, and several doping strategies have been devised, including substitutional doping,[8,9] molecular adsorption,[10-14] covalent functionaliztion,[15-18] substrate surface modification[19-23]and the use of metallic thin films or nanoparticles.[24-26,39,40]

However, the doping strength of these doping method is limited by insufficient charge-transfer from dopants and by electron scattering from substituted atoms leading to low carrier mobility and conductivity. Previously, the chemical doping of graphene has been mainly carried out by coating graphene with dopants or transferring graphene on dopant layers. For example, self-assembled monolayers (SAMs) have been utilized as ultrathin and uniform graphene-doping layers functionalized on an oxide surface,[22,26] which is advantageous because of its simple fabrication process applicable to various surface and interface engineering.[22,27-29] However, the SAM doping on a single-side of graphene did not provide enough doping strength to improve the electrical conductivity of graphene. As the amount of transferred charge is proportional to the surface area of graphene in contact with dopants, simultaneous doping on the dual-side of graphene would be more efficient to enhance the electrical properties of graphene. Here, we demonstrate a simple method to tune the electrical properties of graphene synthesized by chemical vapor deposition (CVD) with dual-side chemical doping – the bottom-side doping via substrate modification with NH_2-SAMs and the top-side doping with diethylenetriamine (DETA) molecules.

Results and discussion

To investigate the electrical properties of the doped graphene, we prepared four different types of graphene field effect transistor samples – top-side, bottom-side and dual-side n-doped graphene and the pristine graphene. Figure 1 shows the schematic views of three types of n-doped graphene devices. To obtain the bottom-side n-doped graphene, NH_2-SAMs was constructed on the surface of SiO_2 (100 nm)/Si substrate by dipping in the aqueous solution of 3-aminopropyltriethoxysilane (volume ratio of 500:1) for 30 minutes. The NH_2-SAMs modified substrate was dried by blowing with nitrogen gun, followed by the careful transfer of graphene onto the substrate. Diethylenetriamine (DETA) was

Nanoscale Accepted Manuscript

This journal is © The Royal Society of Chemistry 2013

used as the top-side n-doping molecule, which exhibits strong n-doping effect.[12] Vapor-phase DETA doping was carried out in the sealed petri-dish from the droplet on tissue under 70 °C baking on a hot plate for 30 minutes. Thus, the dual-side doping with DETA/NH_2-SAMs were completed as shown in Figure 1b, where the two types of dopants including the lone pair electrons of amine functional groups are efficiently positioned to maximize the electron doping effect on both sides of graphene.

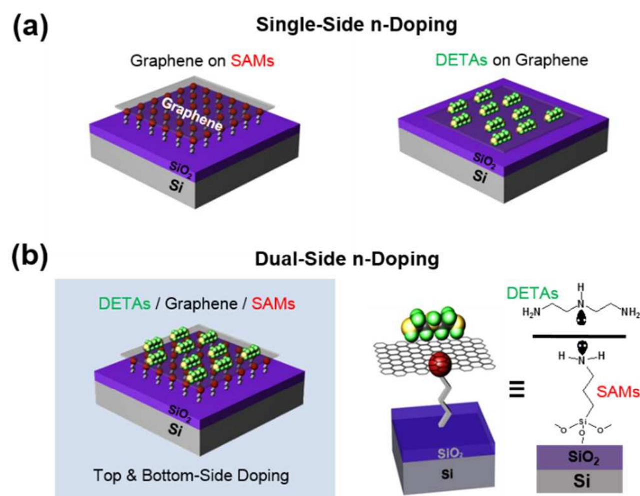

Figure 1. Schematic views of three different types of n-doped graphene. (**a**) Single-side doped graphene: Top-side n-doping (left) with evaporated DETA molecules and bottom-side n-doping (right) with amine-functionalized SAMs. (**b**) Dual-side doped graphene (left) and graphical representation of the molecular structure of the dopants on the both sides of graphene (right).

Figure 2a shows the Raman spectra of the pristine, single-side, and dual-side doped graphene with NH_2-SAMs and DETA. The G band of graphene were up-shifted from 1585 cm^{-1} (pristine) to 1588 cm^{-1} (NH_2-SAMs modified) and 1590 cm^{-1} (DETA doped) and 1600 cm^{-1} (DETA/NH_2-SAMs modified) due to the effect of the Fermi level shift on the phonon frequencies as a result of electron doping.[30]

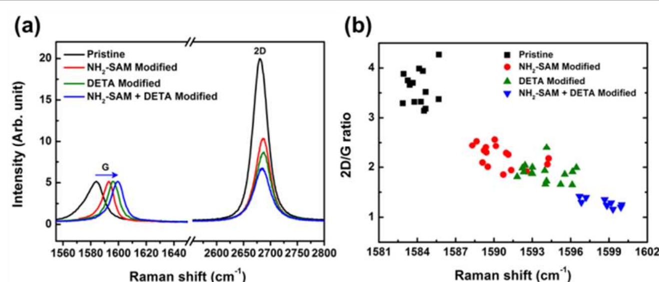

Figure 2. (**a**) The representative Raman spectra of graphene with different dopants (pristine, NH_2-SAMs, DETA and DETA/NH_2-SAMs). (**b**) Raman shift vs. I(2D)/I(G) ratio plot of pristine, NH_2-SAMs modified, DETA doped, and dual-side modified (DETA/NH_2-SAMs) graphene

Noticeably, the intensity ratio of I(2D)/I(G) was also decreased from 3.6 ± 0.3 to 2.2 ± 0.2 for the DETA doped graphene, 1.9 ± 0.2 for the NH_2-SAMs doped graphene, and 1.3 ± 0.1 for dual-side modified graphene (Figure 2b) with the up-shift of G band when chemical doping was applied. This blue shift of G band and the decreased ratio of I(2D)/I(G) exhibit characteristics of typical electron doping of graphene, which has been shown in previous reports.[30-32] Therefore, we confirmed that our doping process successfully induced strong n-doping of graphene.

In Figure 3b, the graphene field effect transistors show different charge neutral points with respect to different doping conditions (schematic shown in Figure 3a). Initially, the charge neutral point (V_{CNP}) of pristine graphene transistors starting at 2 V was negatively changed to -40 V in the bottom-side doped graphene device with NH_2-SAMs. The point was shifted more down to -68 V in the dual-side doped graphene devices modified with DETA/NH_2-SAMs on the both sides of graphene films. The charge neutral point of graphene devices was also shifted to -48 V after top-side doping with DETA (Figure 3c). The mobility of graphene devices can be extracted from the following equation:

$$\mu = \frac{1}{C_i}\frac{d\sigma}{dV_G}$$

where C_i is capacitance of 100 nm SiO_2 (3.24×10^{-8} $F\cdot cm^{-2}$), σ is conductivity of graphene, and V_G is applied gate voltage.

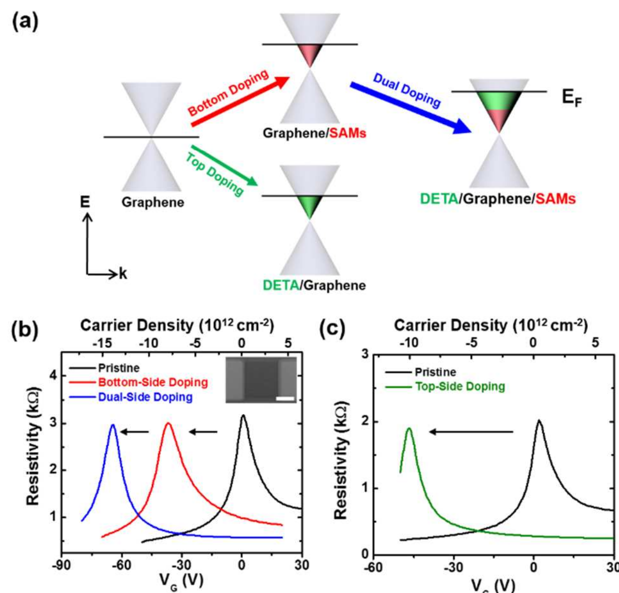

Figure 3. (**a**) Schematic illustration of Fermi energy level (E_f) diagram of different types of n-doped graphene. All the doping processes (bottom-side, top-side and dual-side n-doping) induce significant up-shift of E_f, in particular, dual-side n-doped graphene has much stronger n-type behavior from the molecular n-doping of bottom-side and top-side. (**b**) Current – gate voltage transfer characteristic of the graphene FETs on pristine, bottom-side, and dual-side doped graphene. The inset shows the SEM image of graphene FETs with 100 μm scale bar. (**c**) Current – gate voltage transfer characteristic of the graphene FETs with pristine and DETA doped graphene.

Nanoscale Accepted Manuscript

This journal is © The Royal Society of Chemistry 2012

Graphene field effect devices show relatively high mobility considering its scales (length: 50-250 μm, width: 250 μm) although the graphene channels possibly include some defects such as grain boundaries, ripples and small cracks.[33,34] While the pristine graphene device shows 2791 $cm^2V^{-1}s^{-1}$ for hole region and 2125 $cm^2V^{-1}s^{-1}$ for electron region, the NH_2-SAM modified graphene devices show 1660 $cm^2V^{-1}s^{-1}$ for electron region and 751 $cm^2V^{-1}s^{-1}$ for hole region. Such discordant tendency between the electron and hole mobility of the NH_2-SAM device was mainly caused by misalignment between electrodes and graphene channels in terms of work-function.[35] It is supposed that the suppression in mobility is originated from inhomogeneous coverage of NH_2-SAMs, leading to charge impurities on graphene channels.[36]

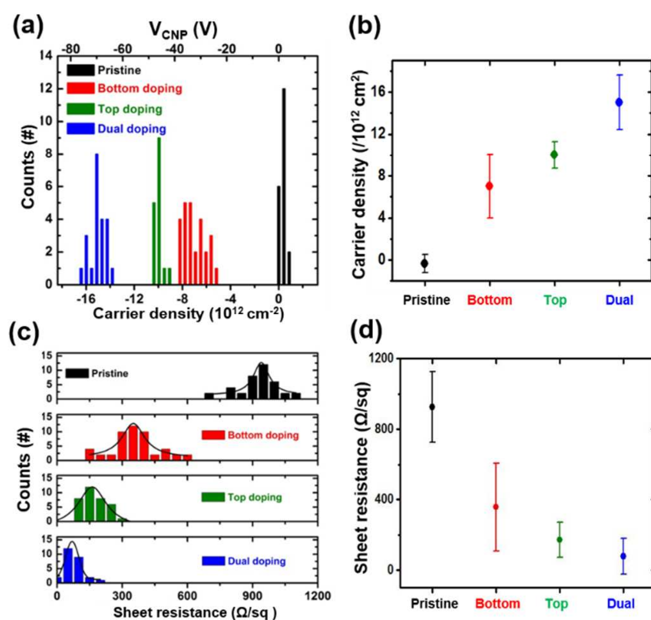

Figure 4. (**a**) Histogram of charge neutral points of graphene FETs doped by NH_2-SAMs, DETA and DETA/NH_2-SAMs (dual-side doped). (**b**) Averages and distributions of carrier density plot of four different types of graphene FETs. (**c**) Histogram of sheet resistance of graphene doped by NH_2-SAMs, DETA and DETA /NH_2-SAMs (dual-side doped). (**d**) Averages and distributions of sheet resistance plot of four different types of graphene FETs.

However, after applying DETA on the top-side of NH_2-modified graphene device, its hole and electron mobility changed to 1775 $cm^2V^{-1}s^{-1}$ and 1808 $cm^2V^{-1}s^{-1}$, respectively. These increased mobility can be explained by the screening effect of charged impurities.[37,38] The top-side doped device with DETA showed 2598 $cm^2V^{-1}s^{-1}$ and 2426 $cm^2V^{-1}s^{-1}$ for hole and electron regions, respectively. In Figure 3c, the schematic diagram represents the tuning of the Fermi level by the chemical doping process. Both bottom-side doping with NH_2-SAM and top-side doping with DETA induced the up-shift of the Fermi level in the case of intrinsic graphene. Interestingly, the dual-side doping resulted in further increased Fermi level, showing much stronger n-doping effect than single-side doping.

To confirm the average molecular doping effect at room temperature, dozens of graphene field effect transistors were measured. The results are plotted as a function of carrier density and charge neutral point in Figure 4a-b. Carrier density is estimated by a typical equation, $n = -\alpha(V_G - V_{CNP})$, with α = 2.16 × $10^{11}cm^{-2}V^{-1}$. We found that the carrier density of graphene was tunable up to -1.7 × 10^{13} cm^{-2} by using dual-side doping, which is the highest value among the recent reports on n-doping of graphene.[23,27,39] To further examine the doping characteristics induced by each dopant, we also measured the sheet resistance of pristine and doped graphene on SiO_2 (100 nm)/Si substrates. The results from more than 30 different positions of graphene are shown in Figure 4c-d. The sheet resistance of graphene gradually decreased from 923 ± 148 Ω/sq, 385 ± 140 Ω/sq, 150 ± 77 Ω/sq and to 86 ± 39 Ω/sq, respectively for pristine, NH_2-SAMs, DETA, and dual-side doped graphene. These results well correspond to the shifts of charge neutral points in the graphene field effect devices, implying that the charge transfer between molecules and graphene can be maximized by increasing the surface area of graphene in contact with n-dopants. The transmittance of dual-side doped graphene measured at 550 nm wavelength is ~96% (Figure S1[‡]).

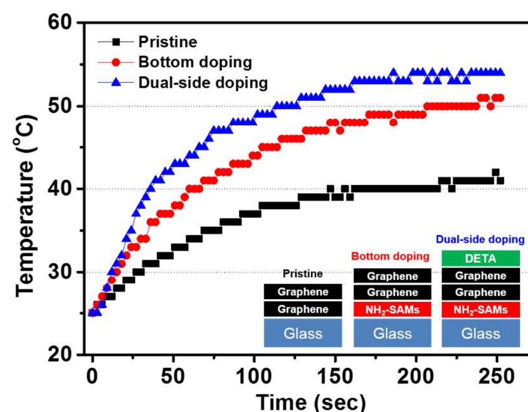

Figure 5. The temperature profiles of pristine, bottom doped and dual-side doped graphene heaters. The size of the heaters was 1.8 x 1.8 cm^2. The temperature responses of the heaters were monitored every three seconds by an infrared camera. The 20 V of input voltage was supplied to the heaters through two-terminal side copper electrodes.

To demonstrate the doping stability, we measured the sheet resistance of the dual-side n-doped graphene after air exposure, thermal heating, and light exposure. The results show that the average sheet resistance was increased by ~20% after 60 min air exposure. After 15 min heating at 70 °C and 100 °C, the sheet resistance was increased to 150 and 350 Ohm/sq, respectively (see details in Figure S2[‡]). In addition, the FET characteristics of DETA-doped graphene with respect to doping time and temperature was also examined (Figure S3[‡]).

Finally, we fabricated transparent heaters based on the n-doped graphene. Figure 5 depicts the time-dependent

Nanoscale Accepted Manuscript

temperature profiles of the graphene-based heaters treated with different dopants. As previously reported, the steady state temperature of the heater depends on the sheet resistance of graphene films.[43] As a result, the dual-side doped graphene heater exhibits the heating temperature as high as 54 °C, while single-side doped and pristine graphene heater show ~51 °C and ~40 °C, respectively (Figure S4‡).

Conclusion

In conclusion, we have developed a simple and efficient dual-side molecular doping method for graphene, demonstrating effective work function modulation, high carrier density (-1.7 × 10^{13} cm^{-2}) and significant reduction of sheet resistance (86 ± 39 Ω/sq), which is believed to be the best conductivity for large-area CVD graphene so far. The actual performance of the dual-side doped graphene film was confirmed by fabricating a transparent heater that exhibits higher heating temperature compared to single-side doped or undoped graphene films. We expect that further efforts to optimize the dual-side doping method would enable wide variety of practical application of graphene films that require low sheet resistance comparable to indium tin oxide (ITO) as well as high transparency and flexibility useful for flexible electronics in the future.[6,12, 22, 40, 41, 43]

Experimental

Sample preparation

Graphene film is synthesized on 25 μm thick copper foil by CVD methods, using mixture of CH_4 (50 sccm) and H_2 (5 sccm) gas as a source with vacuum pumping at 1000 °C. Transfer process of graphene is followed by conventional process: PMMA is spin-coated on top of graphene and then copper foil etched with ammonium persulfate solution (20 mM with distilled water). Highly P-doped Si substrate covered with 100 nm thickness of SiO_2 is used for electrical measurement of graphene field effect devices. Free-standing graphene on distilled water is carefully transferred on bare SiO_2/Si and NH_2-SAMs modified SiO_2/Si substrate respectively and PMMA is removed by using acetone.

Cr (5 nm) and Au (30 nm) are deposited thermally for metal contact of 3-terminal graphene device with using pre-patterned stencil mask. Graphene channels are isolated with electron beam lithography technique. To avoid deviation in growth condition, we use same graphene sample grown in same bath. Each device has as large scales as 250 μm width and 50-250 μm length. Before doping the graphene film, thermal annealing is carried out at 300 °C for 1h with Ar and H_2 gas environment to remove PMMA residues and trapped water after graphene device fabrication process. For UV-Vis measurement and graphene heater, the same n-doping method was applied to a transparent substrate (glass). In case of graphene heater, 2 layer of graphene was used to obtain uniform heating.

Characterization

The n-type doping characteristics of graphene are defined by micro-Raman spectra using a 1mW, 514 nm Ar laser with a spot size of 2 μm (Renishaw inVia Raman microscope). The transmittance was measured by Scinco s-3100 UV-Vis spectrometer. Four types of graphene-based field effect transistors are fabricated to measure the difference of the electrical performances. Agilent 2602 was used on 3-terminal geometry with source, drain and gate. Constant 10 mV voltage applied source to drain during the measurement and sweep range of gate voltage was -80 V to +70 V. The sheet resistance of graphene (0.2 mm × 0.2 mm square geometry) was measured using a four-point probe with a nanovoltmeter (Keithley 6221, 2182A) based on van der Pauw method considering

$$R_s = \frac{\pi}{\ln 2}\frac{V}{I}$$

where R_S is sheet resistance, V is applied voltage and I is current. The temperature responses of the heaters were measured by an infrared camera.[43]

Acknowledgements

This work was supported by the Global Research Lab (GRL) Program (2011-0021972), the Global Frontier Research Program (2011-0031627) and the Basic Science Research Program (2012M3A7B4049807) through the National Research Foundation of Korea (NRF) funded the Ministry of Science, ICT and Future Planning, Korea

Notes and references

[a] Department of Chemistry, Seoul National University, 1 Gwanak-ro, Seoul 151-742, Korea. E-mail: byunghee@snu.ac.kr
[b] Department of Physics & Astronomy, Seoul National University, 1 Gwanak-ro, Seoul 151-742, Korea.
[c] Center for Nanometrology, Korea Research Institute of Standards and Science, Gajeong-Ro, Daejon 305-340, Korea.
[d] School of Physics and Astronomy, University of Manchester, M13 9PL Manchester, United Kingdom.
[e] Sungkyunkwan Advanced Institute of Nanotechnology (SAINT), Sungkyunkwan University, Seobu-ro, Suwon 440-746, Korea.

† These authors contributed equally to this work.
‡ Online supporting information is available.

1. K. S. Novoselov, A. K. Geim, S. V. Morozov, D. Jiang, Y. Zhang, S. V. Dubonos, I. V. Grigorieva and A. A. Firsov, *Science*, 2004, **306**, 666-669.
2. Y. Lee, S. Bae, H. Jang, S. Jang, S.-E. Zhu, S. H. Sim, Y. I. Song, B. H. Hong and J.-H. Ahn, *Nano Lett.*, 2010, **10**, 490-493.
3. K. I. Bolotin, K. J. Sikes, Z. Jiang, M. Klima, G. Fudenberg, J. Hone, P. Kim and H. L. Stormer, *Solid State Commun.*, 2008, **146**, 351-355.
4. R. R. Nair, P. Blake, A. N. Grigorenko, K. S. Novoselov, T. J. Booth, T. Stauber, N. M. R. Peres and A. K. Geim, *Science*, 2008, **320**, 1308.
5. A. A. Balandin, S. Ghosh, W. Bao, I. Calizo, D. Teweldebrhan, F. Miao and C. N. Lau, *Nano Lett.*, 2008, **8**, 902-907.
6. Q. Bao, K. P. Loh, *ACS Nano*, 2012, **6**, 36773694.

Nanoscale Accepted Manuscript

This journal is © The Royal Society of Chemistry 2012

7. S. Bae, H. Kim, Y. Lee, X. Xu, J.-S. Park, Y. Zheng, J. Balakrishnan, T. Lei, H. Ri Kim, Y. I. Song, Y.-J. Kim, K. S. Kim, B. Ozyilmaz, J.-H. Ahn, B. H. Hong and S. Iijima, *Nat. Nanotechnol.*, 2010, **5**, 574-578.
8. L. S. Panchakarla, K. S. Subrahmanyam, S. K. Saha, A. Govindaraj, H. R. Krishnamurthy, U. V. Waghmare and C. N. R. Rao, *Adv. Mater.*, 2009, **21**, 4726-4730.
9. D. Wei, Y. Liu, Y. Wang, H. Zhang, L. Huang and G. Yu, *Nano Lett.*, 2009, **9**, 1752-1758.
10. F. Schedin, A. K. Geim, S. V. Morozov, E. W. Hill, P. Blake, M. I. Katsnelson and K. S. Novoselov, *Nat. Mater.*, 2007, **6**, 652-655.
11. S. Ryu, L. Liu, S. Berciaud, Y.-J. Yu, H. Liu, P. Kim, G. W. Flynn and L. E. Brus, *Nano Lett.*, 2010, **10**, 4944-4951.
12. Y. Kim, J. Ryu, M. Park, E. S. Kim, J. M. Yoo, J. Park, J. H. Kang and B. H. Hong, *ACS Nano*, 2014, **8**, 868-874.
13. Y. Kim, J. M. Yoo, H. Jeon, and B. H. Hong, *Phys. Chem. Chem. Phys.,* 2013, **15**, 18353-18356.
14. X. Dong, D. Fu, W. Fang, Y. Shi, P. Chen and L.-J. Li, *Small*, 2009, **5**, 1422-1426.
15. S. Niyogi, E. Bekyarova, M. E. Itkis, H. Zhang, K. Shepperd, J. Hicks, M. Sprinkle, C. Berger, C. N. Lau, W. A. deHeer, E. H. Conrad and R. C. Haddon, *Nano Lett.*, 2010, **10**, 4061-4066.
16. J. M. Englert, C. Dotzer, G. Yang, M. Schmid, C. Papp, J. M. Gottfried, H.-P. Steinrück, E. Spiecker, F. Hauke and A. Hirsch, *Nat. Chem.*, 2011, **3**, 279-286.
17. B. Guo, Q. Liu, E. Chen, H. Zhu, L. Fang and J. R. Gong, *Nano Lett.*, 2010, **10**, 4975-4980.
18. D. Usachov, O. Vilkov, A. Grüneis, D. Haberer, A. Fedorov, V. K. Adamchuk, A. B. Preobrajenski, P. Dudin, A. Barinov, M. Oehzelt, C. Laubschat and D. V. Vyalikh, *Nano Lett.*, 2011, **11**, 5401-5407.
19. D. Wei, Y. Liu, Y. Wang, H. Zhang, L. Huang and G. Yu, *Nano Lett.*, 2009, **9**, 1752-1758.
20. R. Wang, S. Wang, D. Zhang, Z. Li, Y. Fang and X. Qiu, *ACS Nano*, 2010, **5**, 408-412.
21. M. Lafkioti, B. Krauss, T. Lohmann, U. Zschieschang, H. Klauk, K. v. Klitzing and J. H. Smet, *Nano Lett.*, 2010, **10**, 1149-1153.
22. Y. y. Wang, Z. h. Ni, T. Yu, Z. X. Shen, H. m. Wang, Y. h. Wu, W. Chen and A. T. Shen Wee, *J. Phys. Chem. C*, 2008, **112**, 10637-10640.
23. J. Park, W. H. Lee, S. Huh, S. H. Sim, S. B. Kim, K. Cho, B. H. Hong and K. S. Kim, *J. Phys. Chem. Lett.*, 2011, **2**, 841-845.
24. K. M. McCreary, K. Pi and R. K. Kawakami, *Appl. Phys. Lett.*, 2011, **98**, 192101-192103.
25. K. Pi, K. M. McCreary, W. Bao, W. Han, Y. F. Chiang, Y. Li, S. W. Tsai, C. N. Lau and R. K. Kawakami, *Phys. Rev. B*, 2009, **80**, 075406.
26. J. H. Chen, C. Jang, S. Adam, M. S. Fuhrer, E. D. Williams and M. Ishigami, *Nat. Phys.*, 2008, **4**, 377-381.
27. S. Huh, J. Park, K. S. Kim, B. H. Hong and S. B. Kim, *ACS Nano*, 2011, **5**, 3639-3644.
28. S. A. DiBenedetto, A. Facchetti, M. A. Ratner and T. J. Marks, *Adv. Mater.*, 2009, **21**, 1407-1433.
29. W. H. Lee, J. Park, Y. Kim, K. S. Kim, B. H. Hong and K. Cho, *Adv. Mater.*, 2011, **23**, 3460-3464.
30. A. Das, S. Pisana, B. Chakraborty, S. Piscanec, S. K. Saha, U. V. Waghmare, K. S. Novoselov, H. R. Krishnamurthy, A. K. Geim, A. C. Ferrari and A. K. Sood, *Nat. Nanotechnol.*, 2008, **3**, 210-215.
31. C. Casiraghi, S. Pisana, K. S. Novoselov, A. K. Geim and A. C. Ferrari, *Appl. Phys. Lett.*, 2007, **91**, 233103-233108.
32. C. Stampfer, F. Molitor, D. Graf, K. Ensslin, A. Jungen, C. Hierold and L. Wirtz, *Appl. Phys. Lett.*, 2007, **91**, 241907-241907-241903.
33. Q.Yu, L. A. Jauregui, W. Wu, R. Colby, J. Tian, Z. Su, H. Cao, Z. Liu, D. Pandey, D. Wei, T. F. Chung, P. Peng, N. P. Guisinger, E. A. Stach, J. Bao, S.-S. Pei, Y. P. Chen, *Nat. Mater*. **2011**, 10, 443–449.
34. P. Y. Huang, C. S. Ruiz-Vargas, A. M. van der Zande, W. S. Whitney, M. P. Levendorf, J. W. Kevek, S. Garg, J. S. Alden, C. J. Hustedt, Y. Zhu, J. Park, P. L. McEuen, D. A. Muller, *Nature* **2011**, 469, 389–392.
35. D. B. Farmer, R. Golizadeh-Mojarad, V. Perebeinos, Y.-M. Lin, G. S. Tulevski, J. C. Tsang and P. Avouris, *Nano Lett.*, 2008, **9**, 388-392.
36. F. Schedin, A. K. Geim, S. V. Morozov, E. W. Hill, P. Blake, M. I. Katsnelson and K. S. Novoselov, *Nat. Mater.*, 2007, **6**, 652-655.
37. T. Ando, *J. Phys.Soc. Jpn.*, 2006, **75**, 074716-074717.
38. S. Adam, E. H. Hwang, V. M. Galitski and S. Das Sarma, *Proc. Natl. Acad. Sci.*, 2007, **104**, 18392-18397.
39. P.-H. Ho, Y.-C. Yeh, D.-Y. Wang, S.-S. Li, H.-A. Chen, Y.-H. Chung, C.-C. Lin, W.-H. Wang and C.-W. Chen, *ACS Nano*, 2012, **6**, 6215-6221.
40. Z. K. Liu, J. H. Li, Z. H. Sun, G. A. Tai, S. P. Lau and F. Yan, *ACS Nano*, 2012, **6**, 810-818.
41. K. S. Kim, Y. Zhao, H. Jang, S. Y. Lee, J. M. Kim, K. S. Kim, J. H. Ahn, P. Kim, J. Y. Choi and B. H. Hong, *Nature*, 2009, **457**, 706-710.
42. J. Kang, D. Shin, S. Bae and B.H. Hong, *Nanoscale*, 2012, **4**, 5527-5537
43. J. Kang, H. Kim, K. S. Kim, S. -K. Lee, S. Bae, J. -H. Ahn, Y. -J. Kim, J. -B. Choi, and B. H. Hong, *Nano Lett.* 2011, **11**, 5154-5158.

Nanoscale Accepted Manuscript